Sorption-Enhanced Steam Reforming of Ethanol on a Novel K–Ni–Cu–Hydrotalcite Hybrid Material

ARTICLE *in* INDUSTRIAL & ENGINEERING CHEMISTRY RESEARCH · MARCH 2014

Impact Factor: 2.59 · DOI: 10.1021/ie5000938

5 AUTHORS, INCLUDING:

Adelino Cunha
University of Porto
24 PUBLICATIONS **381** CITATIONS
SEE PROFILE

yi-jiang wu
East China University of Science and Techn…
12 PUBLICATIONS **136** CITATIONS
SEE PROFILE

Alírio E Rodrigues
University of Porto
686 PUBLICATIONS **12,706** CITATIONS
SEE PROFILE

I&EC research
Industrial & Engineering Chemistry Research

Article

pubs.acs.org/IECR

Sorption-Enhanced Steam Reforming of Ethanol on a Novel K−Ni−Cu−Hydrotalcite Hybrid Material

Adelino F. Cunha,*[,†] Yi-Jiang Wu,[†] Ping Li,[‡] Jian-Guo Yu,[‡] and Alirio E. Rodrigues[†]

[†]Laboratory of Separation and Reaction Engineering, Associated Laboratory LSRE/LCM, Department of Chemical Engineering, Faculty of Engineering, University of Porto, Rua Dr. Roberto Frias s/n, 4200-465 Porto, Portugal

[‡]State Key Laboratory of Chemical Engineering, College of Chemical Engineering, East China University of Science and Technology, Shanghai 20037, China

ABSTRACT: A multifunctional K−Ni−Cu−hydrotalcite hybrid material was synthesized for hydrogen production via sorption-enhanced steam reforming of ethanol. The hydrotalcite material was used as support for the incorporation of nickel and copper, both used as active catalytic phases. This material was studied for its catalytic properties for steam reforming of ethanol; it was found that Cu preferentially catalyzes ethanol dehydrogenation and water−gas shift reactions, while Ni is more suitable for acetaldehyde decomposition and steam reforming of methane. It was found that Ni and Cu formed a $Ni_{0.5}Cu_{0.5}$ alloy with the advantage of ensemble formation. Also, promising carbon dioxide adsorption capacity of the material was obtained. The potassium promoter together with the hydrotalcite material for carbon dioxide adsorption ensured a successful sorption-enhanced reaction process. High-purity hydrogen stream (99.8 mol % on dry basis) was obtained during the prebreakthrough period at 773 K with a water-to-ethanol molar ratio of 10 in the feed; the concentration of hydrogen then decreased to 67.1 mol % after the breakthrough period.

1. INTRODUCTION

Energy demands and environmental impacts are major concerns of civilization since the past century.[1] As a result, a new concept of "hydrogen economy",[2] where hydrogen is used as a universal energy carrier, has been proposed.

Several most commonly employed processes such as steam reforming,[3] oxidative reforming,[4] and the combination autothermal reforming[5] can be used to produce hydrogen from different sources[6] such as natural gas, naphtha, and other renewable feedstocks such as ethanol.[7] Among these processes, steam reforming can produce the highest amount of hydrogen from the renewable ethanol feedstock, where ethanol reacts with water steam to produce carbon dioxide and hydrogen. The overall reaction of steam reforming of ethanol (SRE) can be written as

$$CH_3CH_2OH(g) + 3H_2O(g) \leftrightarrow 6H_2(g) + 2CO_2(g)$$
$$\Delta H^0_{298K} = +173.3\ kJ{\cdot}mol^{-1} \quad (1)$$

However, other side reactions also exist.[8] The major challenge is to produce high-purity hydrogen with CO content in parts per million (ppm) level for its application in fuel cells.[9] The sorption-enhanced reaction process (SERP) was regarded as a promising method to produce pure H_2 in a single step and has been extensively studied.[10−13] This concept is the combination of reaction and adsorption in a single column packed with a mixture of catalyst and adsorbent. In order to achieve good dispersion of the catalyst along the column, hybrid multifunctional materials consisting of a selective carbon dioxide adsorption support material and catalytic phase has been developed in some recent studies.[14−18] It was found that hybrid material with nickel as the active phase and hydrotalcite-like compounds (HTlc) as the CO_2 adsorbent[19] can improve the yield of H_2 and the thermal efficiency of the SRE process.[14] However, reaction performance of this hybrid material can be further improved on this nickel-based catalyst. Previous studies have found that nickel-based catalysts favor the methanation reaction,[20] which can lead to a low H_2 yield. Fortunately, it has been proved that copper can restrain the reaction by suppressing the CO dissociation step on Ni,[21] which is the rate-determining step of the methanation reaction. As a result, copper, which has also been regarded as an excellent active phase for water−gas shift reaction (WGS)[22] as well as SRE,[23,24] was employed to improve the H_2 yield.

On the other hand, potassium promoter[25] has been used to enhance the CO_2 adsorption performance on the HTlc material. In this work, where HTlc has been used as the support, the possible acid sites would be Al_2O_3, due to the high aluminum content in the unpromoted material.[26] As an acidic support, Al_2O_3 has the disadvantage of favoring ethanol dehydration reaction to produce the ethylene byproduct,[27] which is considered as the source of graphite/coke[28] that can deposit on the catalyst and causes catalyst deactivation. It has been found that the presence of alkaline metal can neutralize the acid sites in the support material and improve the selectivity toward hydrogen.[29,30]

The major challenge is to combine HTlc with potassium for carbon dioxide uptake and with nickel−copper active phases for the catalytic SRE reaction to achieve SERP. In the present work, a K−Ni−Cu−HTlc hybrid system has been prepared by a simple synthesis method. During the thermal treatment of the

Received: January 8, 2014
Revised: February 14, 2014
Accepted: February 17, 2014
Published: February 17, 2014

   dx.doi.org/10.1021/ie5000938 | *Ind. Eng. Chem. Res.* 2014, 53, 3842−3853

precursor, oxygen and NO_x were released, which were responsible for simultaneous volatile expansion of the material surface and calcination.[14,23,25] Afterward, the material consisting of K_2O, NiO and CuO, together with HTlc, was reduced in a hydrogen atmosphere.

The synthesized hybrid material was systematically studied for its performance. Effects of operating conditions on the activity and selectivity for hydrogen production from SRE with nickel and copper as active catalyst phase were investigated. The carbon dioxide adsorption capacity was further examined by carrying out carbon dioxide breakthrough tests in a fixed-bed reactor with a feed of helium, carbon dioxide, and steam. Finally, the synthesized hybrid material with a K-promoted HTlc structure was also analyzed by selective carbon dioxide sorption for hydrogen production via sorption-enhanced steam reforming of ethanol (SE-SRE).

To the best of our knowledge, there is no similar report in literature discussing the production of hydrogen from ethanol in the presence of such a hybrid system, with nickel and copper as the active catalytic phase coupled with K-promoted HTlc as the support material and carbon dioxide adsorbent.

2. EXPERIMENTAL SECTION

2.1. Synthesis of Hybrid Material. A commercial hydrotalcite-like compound (HTlc), also known as layered double hydroxide (LDH), from Condea (now Sasol), with the designation Pural MG30 (aluminum magnesium hydroxide, with 70 mol % Al_2O_3) was used as support material for potassium, nickel, and copper. The selective carbon dioxide sorbent was mixed with potassium nitrate, nickel nitrate hexahydrate, and copper nitrate trihydrate. The novel preparation method developed in our research group can be found in previous publications.[14,23,25]

Previous studies found that high catalytic performance for SRE can be obtained when a mass ratio of Cu/Ni = 1 is used,[31,32] while promising CO_2 adsorption performance was achieved on HTlc with 20 wt % K-promoter.[33] Therefore, the material prepared is designated by the compounds used (K−Ni−Cu−HTlc) and the corresponding loadings were 20 wt % for K, 5 wt % for Ni, and 5 wt % for Cu. The abbreviation HTlc stands for the Pural MG30 sample used. The calculated amounts of KNO_3, $Ni(NO_3)_2{\cdot}6H_2O$, and $Cu(NO_3)_2{\cdot}3H_2O$ were dissolved in 200 mL of distilled water at room temperature. Hereafter, the pellets of the Pural MG30 sorbent were added to this solution and treated under a heated ultrasonic environment at 373 K for 2 h. The obtained suspension was further dried in an oven at 383 K for 48 h. These materials were smashed and crushed in a grinding mill into a fine powder and then loaded into the reactor for thermal treatment for 48 h at 723 K under a nitrogen flow rate of 50 $N{\cdot}cm^3{\cdot}min^{-1}$. Finally, this system was activated with a pure hydrogen flow rate of 30 $N{\cdot}cm^3{\cdot}min^{-1}$ at 723 K for 24 h.

2.2. Characterization of Hybrid Material. The synthesized material was characterized after activation with hydrogen and before SRE reaction and adsorption tests, by applying different physicochemical techniques.

The elemental composition of the material was determined with inductively coupled plasma optical emission spectrometry (ICP-OES) analysis on an Arcos FHS12 (Spectro Analytical Instruments, Kleve, Germany). The specific surface area of the material was calculated by the Brunauer−Emmett−Teller (BET) method from the nitrogen equilibrium adsorption isotherms at 77 K, determined with ASAP2020-M (Micromeritics Instrument, Atlanta, GA). X-ray powder diffraction (XRD) patterns were recorded within the range 10−80° (2θ) by D/max 2550 V (Rigaku, Tokyo, Japan) diffractometer equipped with a Cu Kα radiation source. The materials were examined with the S-4800 (Hitachi, Tokyo, Japan) scanning electron microscope (SEM).

2.3. Reaction Studies on Hybrid Material. Reaction studies were carried out in a 42 cm long tubular stainless steel fixed-bed continuous down-flow reactor (i.d. = 3.3 cm). The continuous down-flow reactor was loaded with 45.1 g of the obtained multifunctional material, the temperature of the bed was measured and ensured by two thermocouples inside the reactor together with a PID temperature controller (Termolab, Fornos Electricos Lda) inside the heating furnace.

Catalytic tests were carried out between 570 and 753 K with intervals around 50 K, and each run was measured for 4 h. During these intervals, the temperature was subsequently increased exclusively in the presence of the carrier gas helium, with a heating rate of 5 $K{\cdot}min^{-1}$, to ensure total absence of product gases formed during the isothermal runs.

An HPLC pump (Merck L-2130) was used to introduce the liquid ethanol−water mixture (previously treated under ultrasonic environment to remove gases such as oxygen dissolved in the liquid) inside the reactor. In most of the experimental runs, the premixed liquid flow rate of ethanol−water was adjusted from 0.05 to 0.5 $mL{\cdot}min^{-1}$ with a molar ratio of 1:10. In a previous study,[14] it was found that hydrogen production with high purity can be done by the use of such a ratio to improve the SE-SRE performance during the prebreakthrough period, while further increase of the ratio can cause a negative effect. The liquid mixture was vaporized and heated in a spider tube inside the upper part of the reactor (21 cm long) to the same temperature as the temperature of multifunctional material inside the lower part of the reactor. The gas stream passed over the material placed inside the lower part of the reactor.

A Dycor ProLine Process mass spectrometer (Ametek, Berwyn) was used to measure all the partial pressures of products in real time. The schematic representation of the experimental units can be found in a previous work.[13]

The activity of the materials was assessed by measuring the conversions of ethanol and water. The percentage conversions of ethanol and water were calculated with the following expressions:

$$X_{EtOH} = \frac{\dot{n}_{EtOH,0} - \dot{n}_{EtOH}}{\dot{n}_{EtOH,0}} \times 100$$

$$X_{H_2O} = \frac{\dot{n}_{H_2O,0} - \dot{n}_{H_2O}}{\dot{n}_{H_2O,0}} \times 100 \quad (2)$$

where $\dot{n}_i$ represents the molar flow rate of species i at the outlet and $\dot{n}_{i,0}$ is the molar flow rate of species i at the inlet. $\dot{n}_i$ is calculated according to the partial pressures of species and the total molar flow rate at the outlet:

$$\dot{n}_i = p_i \sum \dot{n}_i \qquad \sum \dot{n}_i = \dot{V}\frac{p}{RT} \quad (3)$$

where $\dot{V}$ represents the volumetric flow rate at the outlet and p and T are the pressure and temperature at the outlet, respectively.

The percentage yields of the products are defined as

dx.doi.org/10.1021/ie5000938 | Ind. Eng. Chem. Res. 2014, 53, 3842−3853

$$Y_i = \frac{\dot{n}_i}{\dot{n}_{\mathrm{EtOH},0}} \frac{\nu_{\mathrm{EtOH}}}{\nu_i} \times 100 \quad (4)$$

where ν_i is the stoichiometric coefficient, $\nu_{\mathrm{EtOH}} = 1$, $\nu_{\mathrm{CO}} = \nu_{\mathrm{CO_2}} = \nu_{\mathrm{CH_4}} = 2$, $\nu_{\mathrm{CH_3CHO}} = 1$, and $\nu_{\mathrm{H_2}} = 6$. The selectivities of the compounds can be obtained by

$$S_i = \frac{Y_i}{X_{\mathrm{EtOH}}} \times 100 \quad (5)$$

The H_2 purity (mole percent) of the gas product and productivity (moles per kilogram per hour) during the SE-SRE period was imposed to determine the prebreakthrough period (H_2 purity >99 mol %) and assess the performance of the SE-SRE process:

$$\mathrm{H_2\ purity} = \frac{\int_0^t \dot{n}_{\mathrm{H_2}}\, \mathrm{d}t}{\int_0^t (\dot{n}_{\mathrm{CO}} + \dot{n}_{\mathrm{CO_2}} + \dot{n}_{\mathrm{H_2}} + \dot{n}_{\mathrm{CH_4}})\, \mathrm{d}t} \times 100 \quad (6)$$

$$\mathrm{H_2\ productivity} = \frac{\int_0^t \dot{n}_{\mathrm{H_2}}\, \mathrm{d}t}{m_{\mathrm{material}} t} \quad (7)$$

In addition, the thermal efficiency[14] of the overall process can be calculated by

$$\eta_{\mathrm{SE\text{-}SRE}} = \frac{\dot{n}_{\mathrm{H_2}} \mathrm{LHV}_{\mathrm{H_2}}}{\dot{n}_{\mathrm{EtOH},0} \mathrm{LHV}_{\mathrm{EtOH}} + Q_{\mathrm{input}} + \dot{n}_{\mathrm{feed},0} \Delta H_{\mathrm{latent}}} \quad (8)$$

where $\dot{n}_{\mathrm{feed},0}$ is the molar flow rate of the feed stream and $\Delta H_{\mathrm{latent}}$ is the latent energy of the feed stream, which can be calculated from the latent energies of ethanol (38.9 kJ·mol^{-1}) and water (40.6 kJ·mol^{-1}). $\mathrm{LHV}_{\mathrm{H_2}}$ (244 kJ·mol^{-1}) and $\mathrm{LHV}_{\mathrm{EtOH}}$ (1329.8 kJ·mol^{-1}) are the lower heating values of hydrogen and ethanol. Q_{input} is the energy input in the reactor, which can be obtained from the enthalpy change:

$$Q_{\mathrm{input}} = H_{\mathrm{out}}(T) - H_{\mathrm{in}}(T) = \sum_i \dot{n}_i H_i(T) - \sum_i \dot{n}_{i,0} H_i(T) + \Delta H_{\mathrm{reg}} \quad (9)$$

where $H_{\mathrm{out}}(T)$ and $H_{\mathrm{in}}(T)$ are the enthalpies of the outlet and inlet streams from the reactor at temperature T, and ΔH_{reg} is the CO_2 regeneration heat. The enthalpy of the inlet and outlet streams depends on the enthalpy of each species i under operating conditions and the amount of each species fed into the column and obtained from the outlet.

3. RESULTS AND DISCUSSION

3.1. Characterization of Hybrid Material. Properties of the sorbent, Pural MG30, used as the support material for potassium, nickel, and copper phases were described in previous works.[25,33] The results obtained are compared with previously used systems.

The metal composition of the multifunctional material, together with other physicochemical properties, can be found in Table 1.

The results obtained from ICP-OES suggest good agreement with the nominal mass percentage values. Water release and decomposition reactions during thermal treatment can be explained by

Table 1. Properties of Prepared K−Ni−Cu−HTlc Material

m_{cat}[a] (g)	45.1
K−Ni−Cu−Mg−Al[b] (mass %)	25:16:11:15:33
S_{BET} ($m^2 \cdot g^{-1}$)	38
$\bar{d}_{\mathrm{pore}}$ (nm)	16
V_{pore} ($cm^3 \cdot g^{-1}$)	0.14

[a]Total mass of catalyst. [b]Metal mass fraction from ICP-OES for reduced materials.

$$\mathrm{Ni(NO_3)_2 \cdot 6H_2O \rightarrow NiO + NO + NO_2 + O_2 + 6H_2O} \quad (10)$$

$$\mathrm{Cu(NO_3)_2 \cdot 3H_2O \rightarrow CuO + NO + NO_2 + O_2 + 3H_2O} \quad (11)$$

$$\mathrm{KNO_3 \rightarrow KNO_2 + {}^1/_2 O_2} \quad (12)$$

$$\mathrm{2KNO_2 \rightarrow K_2O + NO + NO_2} \quad (13)$$

The release of the NO_x species together with O_2 improved the volatile expansion of the material (higher surface area and better dispersion) and calcination in a single step.

The N_2 adsorption isotherm of the activated K−Ni−Cu−HTlc hybrid material is given in Figure 1. The shapes of the

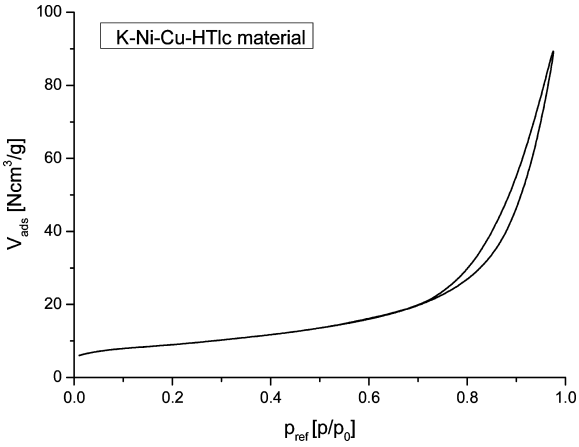

Figure 1. N_2 adsorption−desorption equilibrium isotherm of prepared K−Ni−Cu−HTlc material at 77 K.

obtained isotherms can be interpreted as IUPAC type IV isotherms associated with hysteresis of type H3. Isotherms of this type are characteristic of mesoporous materials, and the average pore sizes of the materials are around 16 nm, similar to the K-promoted HTlc material.[25] In addition, it must be pointed out that this type of hysteresis is related to the aggregates of platelike particles,[34] because the Pural MG30 sample used in this work as sorbent and as support material has such a layered structure.

When the BET surface area of K−Ni−Cu−HTlc hybrid material is compared with those of previously used materials,[14,23,25] it is clear that a subsequent decrease in surface area can be observed. The physicochemical properties of this prepared material were found to be closer to those of the K-promoted HTlc sample, while the physicochemical properties of other hybrid materials (Ni-based[14] or Cu-based[24]) without K promoters were found to be close to the properties of Pural MG30.[26] HTlc MG30, with a 100% available surface area of

dx.doi.org/10.1021/ie5000938 | Ind. Eng. Chem. Res. 2014, 53, 3842−3853

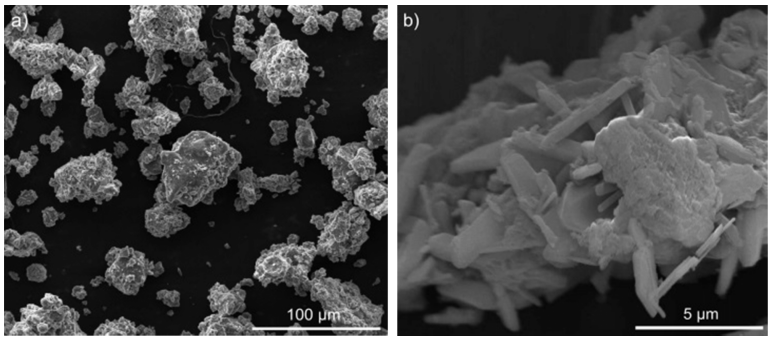

Figure 2. SEM micrographs of prepared K−Ni−Cu−HTlc material.

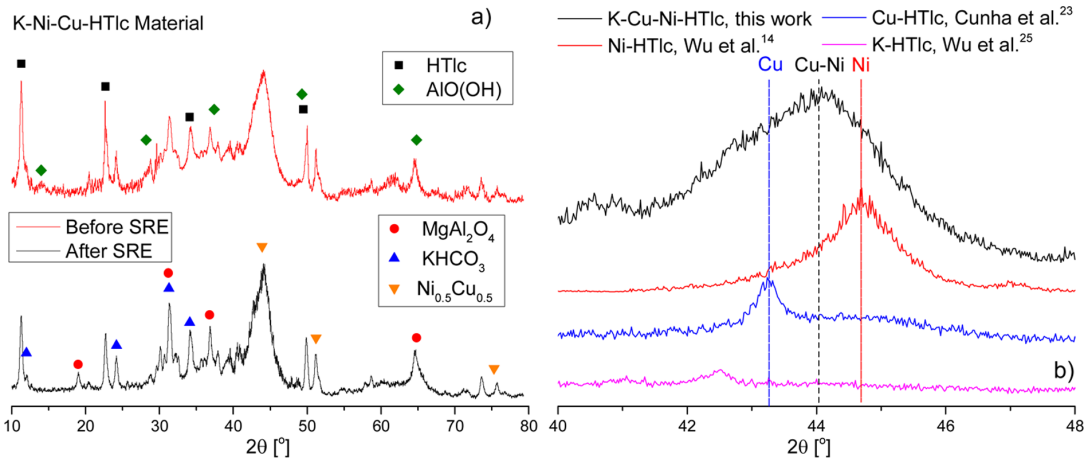

Figure 3. (a) XRD patterns of K−Ni−Cu−HTlc material before and after SRE tests. (b) Comparison of K-HTlc,[25] Ni-HTlc,[14] Cu−HTlc,[23] and K−Ni−Cu−HTlc material synthesized for this work.

200 $m^2 \cdot g^{-1}$, decreases in its surface area to 76% after loading with Ni,[14] to 75% after loading with Cu,[24] and to 14.5% after incorporation of the K promoter.[25] The percentage of the surface area decrease for the K−Ni−Cu−HTlc hybrid material was 19% (this work). The average pore diameter obtained for the K−Ni−Cu−HTlc hybrid material (16 nm) was also in good agreement with values for previously used materials (between 8 and 15 nm). On the other hand, the pore volume of the hybrid material (0.14 $cm^3 \cdot g^{-1}$) was in the range of the value for potassium-promoted HTlc,[25] which is reasonable since the loadings are similar. For HTlc materials incorporating nickel[14] and copper,[24] the pore volumes were 0.31 and 0.32, respectively, since the metal loadings of these materials were much smaller (~5 wt %).

As previously mentioned, the adsorption−desorption isotherm indicated that the material was mostly composed by platelike particles, as shown in the SEM micrograph depicted in Figure 2. In previously published studies,[14,23,25] the same morphology was also observed. From Figure 2, it is clear that the morphology was kept for the K−Ni−Cu−HTlc hybrid material, while the diameter of the multifunctional material particle varies from 30 to 50 μm.

XRD patterns of the synthesized hybrid material before and after SRE tests can be found in Figure 3, and Table 2 lists the bulk phases with corresponding 2θ positions.

Table 2. Phases Identified in K−Ni−Cu−HTlc with Corresponding 2θ Positions

phase	2θ positions (reflection planes)	ICDD PDF no.[a]
$Mg_6Al_2(CO_3)(OH)_{16}\cdot 4H_2O$	11.3° (006), 22.7° (018), 34.4° (024), 48.9° (211)	41-1428
$MgAl_2O_4$	19.0° (111), 31.2° (220), 36.8° (311), 65.2° (440)	77-1193
$KHCO_3$	12.0° (200), 24.2° (400), 31.3° (111), 34.1° (41-1)	89-2369
$Ni_{0.5}Cu_{0.5}$	44.5° (111), 51.8° (200), 76.4° (220)	70-1849
AlO(OH)	14.0° (010), 28.2° (110), 37.4° (111), 49.3° (210), 65.0° (002)	49-0133

[a]International Centre for Diffraction Data powder diffraction file number.

The material reduced before SRE consisted of multiphase compositions and had the presence of boehmite [AlO(OH)], potassium bicarbonate ($KHCO_3$), and HTlc material [$Mg_6Al_2(CO_3)(OH)_{16}\cdot 4H_2O$], as expected. However, the 2θ positions of the characteristic reflections corresponding to the Ni phase at 44.5° [powder diffraction file (PDF) 70-1849] and Cu phase at 43.4° (PDF 65-9743) cannot be distinguished, because a strong overlapping peak can be observed between the 2θ positions from 41° to 47.5°. Previous researches have shown that a strong overlapping peak can be found only when a well-formed Ni−Cu alloy is obtained;[35] otherwise, two separated

dx.doi.org/10.1021/ie5000938 | Ind. Eng. Chem. Res. 2014, 53, 3842−3853

peaks can be found when an incipient alloy is synthesized[36] or a physical mixture is prepared.[35] Besides, the alumina (PDF 29-0063) content did not appear since the strongest peak for this material at 67° was not found. Therefore, the results from XRD in this work clearly indicated the formation of a nickel−copper alloy ($Ni_{0.5}Cu_{0.5}$). These results are in agreement with a former report by Cunha et al.,[37] where the formation of nickel−copper alloys has been studied thoroughly.

On the other hand, it can be seen from samples before and after SRE that most of the HTlc structure was kept during the SRE tests. Only traces of magnesium aluminum oxide ($MgAl_2O_4$) were detected (2θ = 19°) after SRE. Due to the high aluminum content, the prepared material contained a significant amount of boehmite;[26] the peaks from boehmite overlapped with the peaks from $MgAl_2O_4$ except the peak at 19°.

As previously calculated from thermodynamic equilibrium,[38,39] carbon deposition can be suppressed with a water-to-ethanol ratio higher than 4. It is in good agreement with the XRD results reported in Figure 3b, since no carbon deposition can be detected due to the relatively high water-to-ethanol molar ratio (10) used in the feed. Another method to avoid carbon deposition and other undesired side reactions is the formation of small ensembles of nickel surface atoms. These small ensembles of surface atoms have the benefit of minimizing interactions of adsorbed species formed during a catalytic process.

For good catalytic activity, small crystal sizes of the active phases are desired. Table 3 collects the crystal sizes of the formed nickel−copper alloy in the hybrid material used for SRE. Additionally, crystal sizes of previously used materials were introduced for comparison purposes.

Table 3. Metal Crystal Sizes[a]

material	d_{Ni} (nm)	d_{Cu} (nm)	d_{NiCu} (nm)
K−Ni−Cu−Mg−Al (this work)	na	na	15
Cu−Mg−Al[23]	na	16	na
Ni−Mg−Al[14]	5	na	na

[a]Obtained from Ni, Cu, and $Ni_{0.5}Cu_{0.5}$ reflections via the Scherrer equation.

The broad peak around 45° indicated a small crystal size obtained for the nickel copper alloy,[40] and the average metal crystal size was found to be 15 nm in the K−Ni−Cu−HTlc hybrid material, which was in approximation with 16 nm obtained from the crystal size of Cu for Cu−HTlc system.[23] This phenomenon is related to incorporation of copper in the nickel lattice and the lower melting point of copper (Tamman and Hüttig criteria).[41]

3.2. Catalytic Performance of Hybrid Material.

3.2.1. Catalytic Activity for Hybrid Material Used under Steady-State Conditions. SRE tests were performed with different feeding rates in a temperature range between 570 and 753 K. Catalytic activity was investigated in terms of ethanol and water conversion. The results obtained with different feeding rates are depicted in Figure 4. Lines were introduced to follow the experimental points, and the results were collected under steady-state conditions, taken within postbreakthrough regions at least after 1 h since the start of reaction, and when the concentrations of the products did not vary more than 5 mol % for at least 5 min. Higher temperatures have not been tested in order to avoid irreversible destruction of the hydrotalcite-like structure at temperatures higher than 773 K.[42] External and intraparticle diffusion limitations were determined (at lowest and highest temperatures) with the Weisz−Prater criterion and Mears' criterion, respectively. It was found that catalytic tests were performed under the kinetic control regime and the effect of external and intraparticle diffusion can be neglected. In addition, it was found that the pressure drop with highest feeding flow rate at 773 K was around 2% of the atmospheric pressure. Therefore, the effect of pressure drop on reaction performance was not considered. Heat transfer effects in the hybrid material particles and temperature gradients in the bed can also be discarded since they were not found.

Previous thermodynamic studies[38,43] found that ethanol is a thermodynamically unstable compound at temperatures higher than 523 K. Therefore, the equilibrium conversion of ethanol was always 100% within the temperature range used in this work. Equilibrium water conversions at three different temperatures are also included in Figure 4 (shown by horizontal dashed lines) according to thermodynamic calculations with real gas model.[39] The conversion of ethanol from the

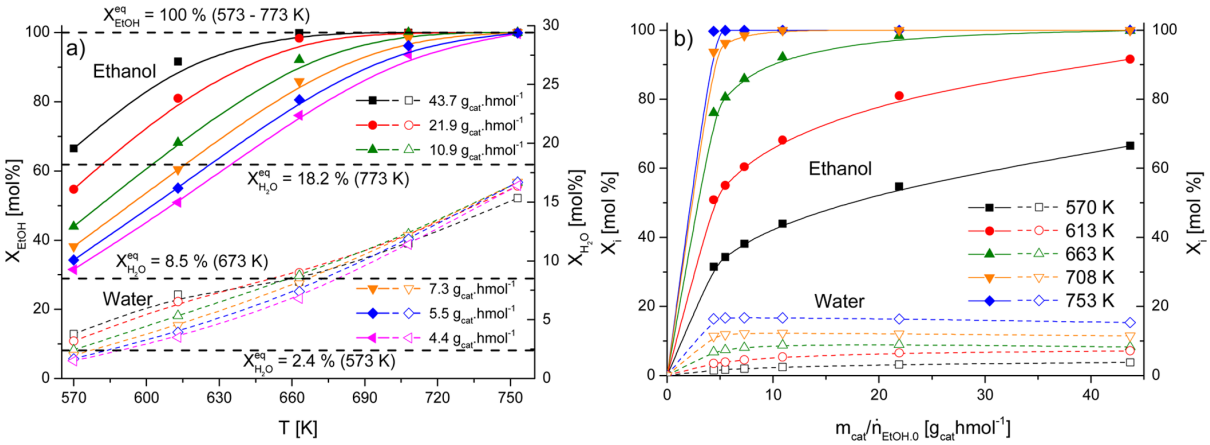

Figure 4. Effect of (a) reaction temperature and (b) contact time on ethanol and water conversions under steady-state conditions, where X_i^{eq} stands for equilibrium conversions of reactants from the thermodynamic study.[36]

dx.doi.org/10.1021/ie5000938 | Ind. Eng. Chem. Res. 2014, 53, 3842−3853

experiments increased with rising reaction temperatures (Figure 4a) and increasing contact times (Figure 4b). According to the reaction scheme given in Table 4, this fact is expected since the

Table 4. Reaction Scheme of Ethanol Steam Reforming

reactions	chemical description	ΔH^0_{298K} (kJ·mol^{-1})
ethanol dehydrogenation (ETD)	$C_2H_6O \leftrightarrow C_2H_4O + H_2$	+68.4
acetaldehyde decomposition (ACD)	$C_2H_4O \leftrightarrow CH_4 + CO$	−18.8
water−gas shift (WGS)	$CO + H_2O \leftrightarrow CO_2 + H_2$	−41.4
steam methane reforming (SMR)	$CH_4 + H_2O \leftrightarrow CO + 3H_2$	+205.9

fast endothermic ethanol dehydrogenation (ETD) reaction[44] is the first reaction step in SRE. Because copper was present as an active catalyst phase, ETD was even more favored.[45] However, conversions of ethanol can decrease with increasing feeding flow rates due to the shorter reaction times.

The conversion of water also increased with increasing temperature (Figure 4a), while the feeding rate of the liquid reactant (contact time, Figure 4b) had a negative effect on the conversions. It is also important to stress that the activation energy of water is higher than that for ethanol, which means higher temperatures are required to convert water. The thermodynamic conversion of water at 773 K with a water-to-ethanol molar ratio ($R_{S/E}$ = 10) used in the feed can reach a maximum of only 18.2%. This phenomenon can be attributed to the thermodynamic equilibrium limitation of the SMR as well as the WGS reaction.[38,39] In these experimental tests, the highest water conversion of around 17% was reached with the K−Ni−Cu−HTlc hybrid material.

With the presence of nickel as active phase, the propensity of activating the endothermic steam methane reforming (SMR) at higher temperature levels can be obtained, while the presence of copper favors the activation of the exothermic WGS.[46] No acetaldehyde was found at a reaction temperature of 753 K, as shown in Figure 5, which is a good indication that nickel is suitable for acetaldehyde decomposition (ACD).[29,47]

It has been observed from XRD results that between nickel and copper an alloy[37] was formed. The formation of small ensembles of nickel and copper atoms on surface can avoid the interaction of adsorbed species,[48] and the catalytic decomposition of methane and catalytic carbon monoxide decomposition can be avoided. The generated carbon monoxide from SMR by the nickel active phase can be converted by the neighboring copper active phase in the WGS reaction. It was also found that the crystal sizes of the Ni−Cu alloy are very small, which can be the explanation for the high activities of the hybrid material synthesized. Finally, there is also a good possibility that the K species used in the hybrid material acted as an electronic promoter for WGS reaction.[49]

3.2.2. Product Distribution for Hybrid Material Used on Dry Basis under Steady-State Conditions. The selectivities of intermediate compounds formed during SRE as a function of reaction temperature in the presence of hybrid material is shown in Figure 5.

The results showed that, at lower temperatures, high selectivity toward acetaldehyde was observed (Figure 5a). The high selectivity toward acetaldehyde suggests a fast ETD, which can be the contribution of the active copper phase,[24] while nickel as the active phase was more responsible for the

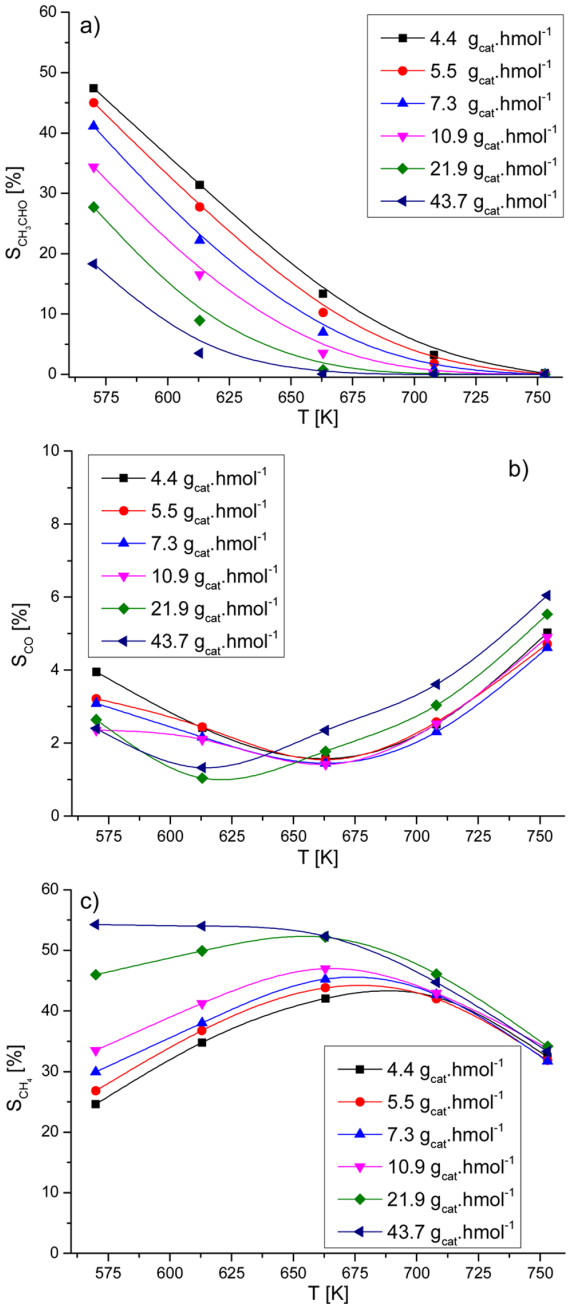

Figure 5. Selectivities of intermediate products at different reaction temperatures and feeding flow rates under steady-state conditions: (a) CH_3CHO, (b) CO, and (c) CH_4.

C−C bond cleavage[50] by catalytic cracking of acetaldehyde into methane and carbon monoxide, known as ACD. These deductions can be confirmed by the selectivities of acetaldehyde and carbon monoxide, which were not the stoichiometric ratio of ETD.

The presence of acetaldehyde decreased strongly with increasing temperature and lower amounts of reactant feeding. It could be an indication that the bimetallic Ni−Cu alloy system improves the ACD reaction.[32] Previous study found that

dx.doi.org/10.1021/ie5000938 | Ind. Eng. Chem. Res. 2014, 53, 3842−3853

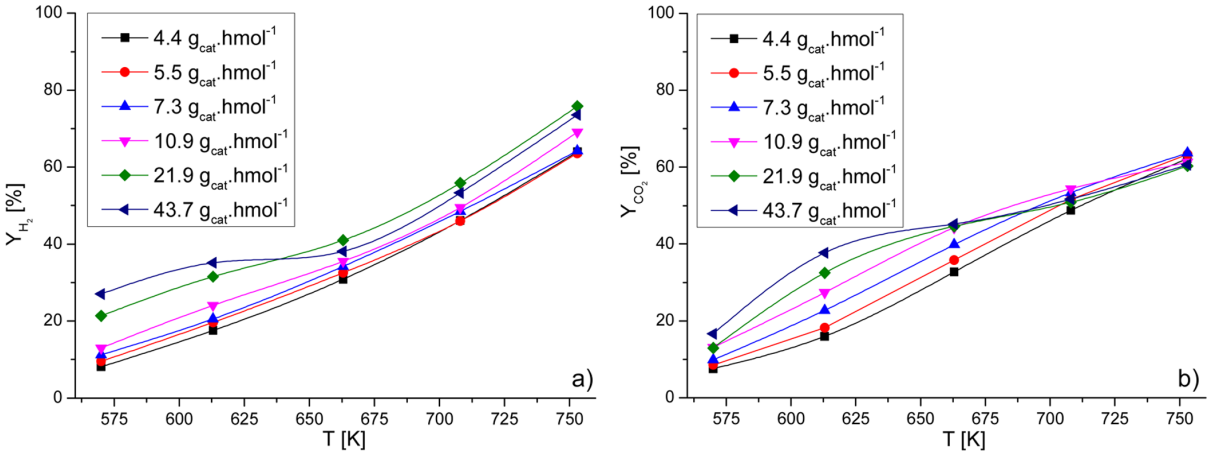

Figure 6. Product yields of (a) H_2 and (b) CO_2 at different reaction temperatures and feeding flow rates under steady-state conditions.

the addition of a second metal (copper) can lead to a promoting effect on Ni for the decomposition of C_2^+ species.[21] The presence of potassium may also electronically promote[51] both ETD and ACD, since the selectivity of acetaldehyde decreased rapidly.

Carbon monoxide appeared with low selectivities (Figure 5b) during all the SRE measurements (less than 6%), which is important for pure hydrogen production. It is also clear that WGS was promoted since the selectivity toward carbon monoxide for the hybrid material used in this work is much lower than for the previously used material (without copper)[14] within the low-temperature region. However, the selectivity of carbon monoxide first decreased with the rise of temperature, reaching a minimum at ~660 K. The result suggested that the forward reaction rate of WGS was higher than ACD at intermediate temperatures, since the lowest selectivity toward carbon monoxide under different feeding flow rates was obtained between 600 and 700 K.

The backward WGS and the backward SRM (known as reverse WGS and methanation reactions) are the main side reactions in SRE, leading to the consumption of hydrogen. In Figure 5c it can be observed that higher reaction temperatures favor SMR due to the thermodynamic equilibrium of this reaction, which is the major reason for the decrease in methane selectivity and increase in hydrogen selectivity. In addition, Cu could suppress the methanation reaction by suppressing the dissociation of CO on the Ni surface.[21] In comparison with a previous study where a Ni−HTlc material[14] was used at 673 K under similar reaction conditions, the selectivity toward methane decreased with the use of Ni−Cu alloy as active phase, from 62% to 45% in this study. On the other hand, the reverse WGS reaction became significant at high temperatures and the selectivity of carbon monoxide increased as methane selectivity decreased. Besides, it was found that the WGS closely reached equilibrium at high temperature conditions, the experimental results from the test performed at 753 K with 4.4 $g_{cat}{\cdot}h{\cdot}mol^{-1}$ (lowest contact time) in the feed was calculated, and the WGS reaction constant from our study (5.71) was close to the equilibrium constant (5.87), while at low temperature (T = 570 K, with the longest contact time 43.7 $g_{cat}{\cdot}h{\cdot}mol^{-1}$) the reaction constant (1.76) was found to be much lower than the equilibrium value at 570 K (42.2).

The yields for hydrogen and carbon dioxide produced during SRE as a function of reaction temperature in the presence of K−Ni−Cu−HTlc hybrid material is shown in Figure 6.

The yield for hydrogen (Figure 6a) increased with rising temperature at different feeding flow rates. The yield of hydrogen with the longest contact time (43.7 $g_{cat}{\cdot}h{\cdot}mol^{-1}$) was found to be highest at low temperatures, because more ethanol can be converted (Figure 4a) into hydrogen and acetaldehyde under the low feeding flow rate condition. Under high-temperature conditions, the effect of contact time became less obvious, since the ethanol reactant and the intermediate product acetaldehyde (Figure 5a) were already converted.

On the other hand, the yield of carbon dioxide (Figure 6b) first increased rapidly with rising temperature, and then the increase slowed down due to the reverse WGS at these conditions. Meanwhile, more carbon monoxide appeared at higher temperatures (Figure 5b).

Finally, for all the reaction conditions used, no carbon deposition was found. Carbon deposition, generated by CO dissociation[52] at low temperatures (<573−648 K), can be suppressed when $R_{S/E} \geq 4$. In addition, a graphitic carbon film appears only at higher temperatures (>873 K) due to thermal cracking of methane.[37] Since SRE tests were carried out between 570 and 753 K, the carbon film formation can be avoided.

3.3. Carbon Dioxide Adsorption Performance of Hybrid Material. Pure hydrogen production for fuel cells can be obtained, for example, by a sorption-enhanced reaction process (SERP). Sorption-enhanced steam reforming of ethanol (SE-SRE) for pure hydrogen production requires a multifunctional material with the ability to capture carbon dioxide selectively, especially when the hybrid material was incorporated with catalytic active phases, as in this work. The influence of the active copper and active nickel phase on carbon dioxide sorption behavior for the hybrid material used in this work was studied and also compared with previous results.[25,33,53] For implementation of the obtained multifunctional material in a SE-SRE study, the CO_2 sorption capacity must be determined at different temperatures.

Sorption isotherms were obtained by measuring the breakthrough curves of carbon dioxide. The measured gas effluent in the breakthrough test was considered at equilibrium when the carbon dioxide concentration at the outlet of the

dx.doi.org/10.1021/ie5000938 | Ind. Eng. Chem. Res. 2014, 53, 3842−3853

column did not vary for at least 5 min. Detailed conditions can be found in Table 5.

Table 5. Operating Conditions Used in Breakthrough Tests

temperature (K)		669, 721, 763
total pressure (kPa)		100
flow rate ($cm^3 \cdot min^{-1}$, 298 K, 100 kPa)		200
material mass (kg)		0.04
p_{CO_2} (kPa)	p_{H_2O} (kPa)	p_{He} (kPa)
	Adsorption	
5	50	45
10	50	40
20	50	30
30	50	20
40	50	10
50	50	0
	Desorption	
0	50	50

The carbon dioxide sorption capacity of the prepared material is defined as

$$q_{CO_2} = \frac{n_{CO_2,adsorbed}}{m_{sorb}} = \frac{\dot{n}_{CO_2,feed} t_s - \int \dot{n}_{CO_2,out}\, dt}{m_{sorb}} \quad (14)$$

where q_{CO_2} is sorption capacity of the material, m_{sorb} is mass of sorbent material, $n_{CO_2,adsorbed}$ is the mole number of adsorbed CO_2 on the hybrid material, $\dot{n}_{CO_2,feed}$ is molar flow rate of CO_2 feed, $\dot{n}_{CO_2,out}$ is molar flow rate of CO_2 at outlet, and t_s is time for stabilization. After CO_2 adsorption and SE-SRE reaction, regeneration was carried out until $\dot{n}_{CO2,out} \leq 0.1$ mmol·min^{-1} without variation for 5 min in the outlet stream with water (p_{H_2O} = 50 kPa), helium (p_{He} = 50 kPa), and a total feed flow rate equal to 200 N·cm^3·min^{-1}. It can be found that, during all the tests, a steam feed with partial pressure of 50 kPa has been used. As had been reported,[53] the adsorption process on an HTlc material in the presence of steam favors CO_2 capture. Furthermore, the layered structure of HTlc can be recovered or maintained when contacted with ambient moisture, which is known as the memory effect.[54] Finally, sorption equilibrium isotherms at 669, 721, and 763 K were measured, as depicted in Figure 7.

The symbols in Figure 7 are the experimental data, and the solid curves correspond to the Langmuir isotherm at different conditions:

$$q_{CO_2} = q_{max} \frac{b_{CO_2} p_{CO_2}}{1 + b_{CO_2} p_{CO_2}} \qquad b_{CO_2} = b_{CO_2,0} e^{-\Delta H_{ads}/RT} \quad (15)$$

where q_{max} = 1.21 mol·kg^{-1} is the theoretical maximum capacity, $b_{CO_2,0} = 2.11 \times 10^{-3}$ kPa^{-1}, and $\Delta H_{ads} = -18.7$ kJ·mol^{-1} is the heat of carbon dioxide adsorption.

The adsorption heat of this material was close to results obtained by Ding and Alpay[53] (−17 kJ·mol^{-1}) on a K_2CO_3-promoted HTlc material under similar conditions. The adsorption capacity was found to be much higher than that of the unprompted NiMgAl sample.[14] The CO_2 adsorption capacity of the hybrid material with K promoter in this study was 0.83 mol·kg^{-1} at 721 K and p_{CO_2} = 40 kPa, while the NiMgAl material has a capacity of 0.26 mol·kg^{-1} at 723 K and p_{CO_2} = 40 kPa. The possible explanation for the improvement on the CO_2 sorption capacity can be found in a previous report.[25] It seems also that the active phases, Ni and Cu, do not influence the sorption behavior of the support material.

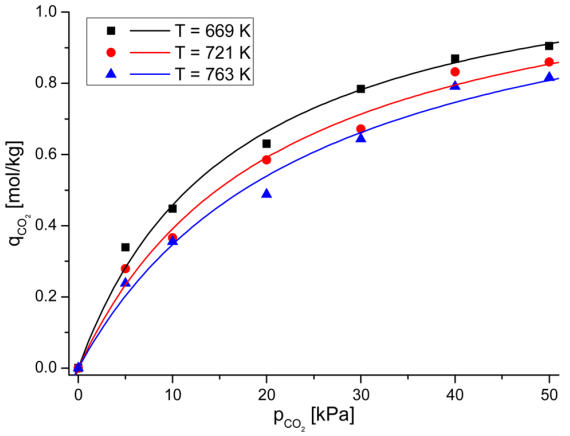

Figure 7. CO_2 adsorption equilibrium isotherms on K−Ni−Cu−HTlc material at 669, 721, and 763 K.

It can be found from the sorption isotherms that the highest carbon dioxide adsorption capacity was obtained at the lowest temperature (669 K), due to the exothermic carbon dioxide adsorption process. However, we cannot simply come to the conclusion that low temperature favors the SE-SRE process, since the operating conditions for a successful SE-SRE process should be established in combination with both promising catalytic and adsorption performance of the hybrid material.

3.4. Sorption-Enhanced Reaction Process. The feasibility of operating regions on SE-SRE for high-purity hydrogen production should be investigated. The K−Ni−Cu−HTlc hybrid material was studied under different reaction conditions. Figure 8 depicts the molar fractions obtained for hydrogen, carbon dioxide, carbon monoxide, and methane at 723 and 773 K for the same contact time during the transient time period and steady-state period.

It is important to note that in this study the highest reaction temperature applied for SE-SRE tests was 773 K, where irreversible HTlc structure destruction can be avoided.[54] In a previous study,[38] it was also found from thermodynamic equilibrium conditions that the performance of SE-SRE benefits from a low-pressure operation, because the overall reaction (eq 1) is a volume increase reaction. Therefore, atmospheric pressure was used during SE-SRE tests.

At a lower temperature, 723 K (Figure 8a), the yield of hydrogen produced during the transient period was relatively lower than at 773 K (Figure 8b). On the other hand, the breakthrough time for methane (and carbon monoxide) was shorter as for a lower temperature. This means that at 723 K mainly SE-WGS occurred, while at 773 K both SE-SMR and SE-WGS were performed simultaneously. As a result, the yield of hydrogen for the latter case was higher and the carbon dioxide breakthrough time was longer. After breakthrough, the outlet concentrations observed under steady-state conditions corresponded to the previously observed SRE experiments (Figures 4−6).

dx.doi.org/10.1021/ie5000938 | Ind. Eng. Chem. Res. 2014, 53, 3842−3853

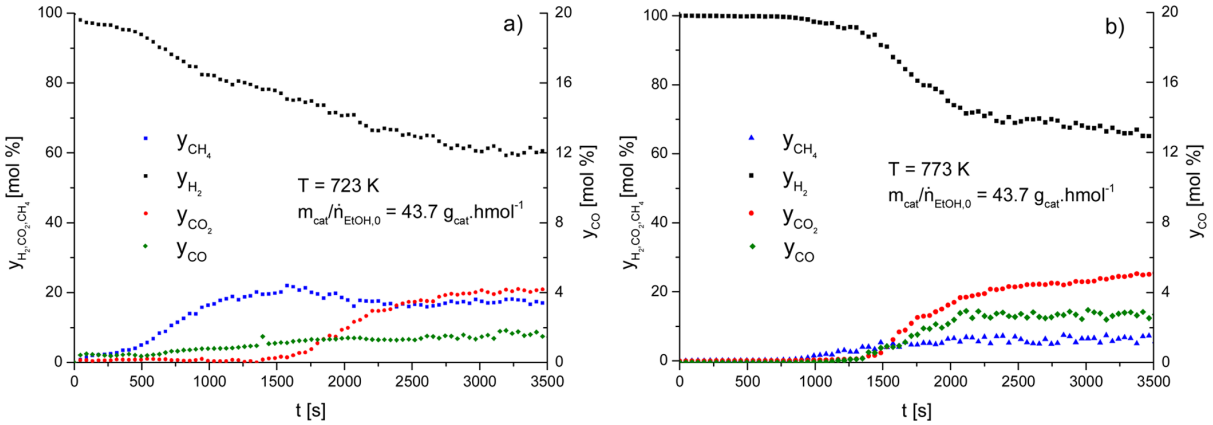

Figure 8. Product distributions as a function of reaction time at (a) 723 K and (b) 773 K for $m_{cat}/\dot{n}_{EtOH,0}$ = 43.7 g_{cat}·h·mol^{-1}.

Table 6. Comparative Performances of Materials Used for SE-SRE and SRE

		prebreakthrough state (SE-SRE)			postbreakthrough state (SRE)		
material	operating conditions	X_{EtOH} (%)	y_{H_2} (mol %)	S_{H_2} (%)	X_{EtOH} (%)	y_{H_2} (mol %)	S_{H_2} (%)
thermodynamic calcn[38]	*a*	100	99.9	98.3	100	66.0	63.0
Co−Ni/HTlc with CaO[59]	*b*	100	>99	na	100	66	na
Ni/Al_2O_3 with Li_4SiO_4[60]	*c*	100	~98	~87	100	~61	~58
Ni/Al_2O_3 with HTlc[13]	*d*	100	98.7	21.8	64.2	56.0	25.1
Cu−HTlc[23]	*d*	100	91.7	24.4	83.8	84.4	22.6
Ni−HTlc[14]	*a*	100	98.2	95.7	100	66.4	66.3
K−Ni−Cu−Mg−Al (this work)	*a*	100	99.8	96.5	100	67.1	66.7

[a] T = 773 K, p = 101 kPa, $R_{S/E}$ = 10. [b] T = 823 K, p = 101 kPa, $R_{S/E}$ = 6. [c] T = 800 K, p = 101 kPa, $R_{S/E}$ = 6. [d] T = 673 K, p = 101 kPa, $R_{S/E}$ = 10.

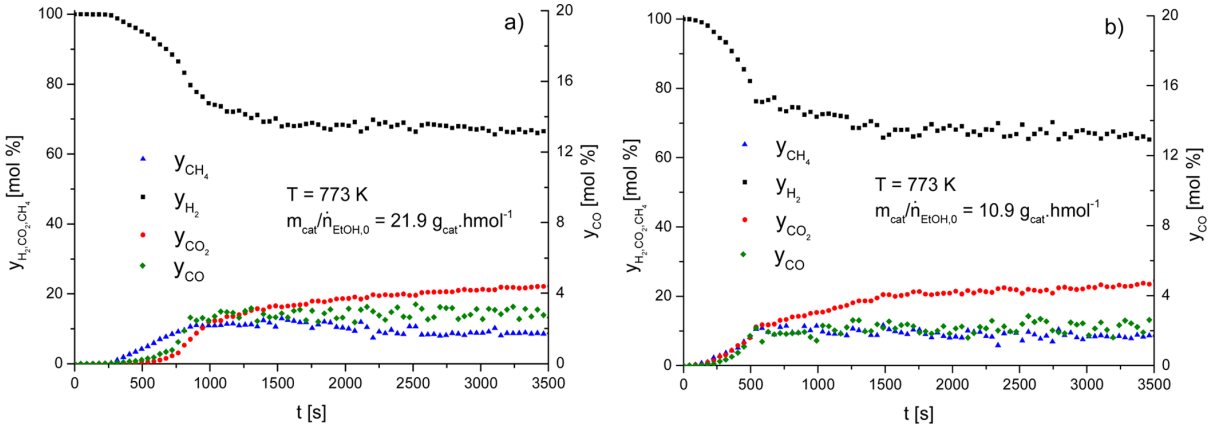

Figure 9. Product distributions as a function of time at 773 K for (a) $m_{cat}/\dot{n}_{EtOH,0}$ = 21.9 g_{cat}·h·mol^{-1} and (b) $m_{cat}/\dot{n}_{EtOH,0}$ = 10.9 g_{cat}·h·mol^{-1}.

In addition, a comparison between the results, both SE-SRE and SRE tests, for prepared K−Ni−Cu−HTlc material and other studies can be found in Table 6, where y_{H_2} (mole percent) represents the concentration of H_2 in the product gas (dry basis). Among the SE-SRE studies published, many pairs of catalyst−sorbent systems have been developed. These configurations can be classified into two groups: alternate layers of catalyst and sorbent or uniform mixtures of the two materials. By packing the bed with several layers of catalyst and sorbent sequentially, the column is just a combination of several reactors and adsorbers in series. The arrangement can affect the overall performance.[55] Rawadieh and Gomes[56] compared different layered systems and found that a well-mixed configuration can produce higher hydrogen purity with lower CO content compared to other layered configurations, which is in agreement with the result found by Lu and Rodrigues.[57] However, in practice it is very difficult to obtain an ideal mixed catalyst−sorbent system due to differences in particle size, shape, and density of the catalyst and sorbent materials. Alternatively, recent studies suggested that a homogeneous mixture can be achieved by synthesis of sorbent material together with an active phase.[14,23,58]

Use of a carbon dioxide adsorbent can improve the hydrogen production performance in the reforming process, since under

dx.doi.org/10.1021/ie5000938 | Ind. Eng. Chem. Res. 2014, 53, 3842−3853

all these different operating conditions, the yields and selectivity of hydrogen were much higher during the prebreakthrough state (sorption-enhanced reaction region) than that obtained from conventional reforming process. According to the results collected from K−Ni−Cu−HTlc material (Table 6), for both the pre- and postbreakthrough periods, the hydrogen concentrations and selectivity were found to be close to thermodynamic calculations for SE-SRE and SRE, respectively. It is an indication of the promising reaction and adsorption performance of the multifunctional material. In addition, hydrogen with a higher concentration can be produced from the use of a K−HTlc material as carbon dioxide sorbent than the other high-temperature carbon dioxide sorbents.

The developed multifunctional material can offer promising H_2 production performance (y_{H_2} = 99.8 mol % and S_{H_2} = 96.5%) during the prebreakthrough region, compared with conventional operation[59,60] of the bed packed with a mixture of catalyst and sorbent. As a result, the development of a multifunctional material can eliminate the use of additional catalyst support and offers the advantage of reducing the reactor size.[58]

SE-SRE with different feeding flow rates has also been performed, as shown in Figure 9. According to calculation of the test shown in Figure 9a, where the prebreakthrough period was 360 s, 0.0144 mol of H_2 was collected at the outlet. Therefore, the H_2 productivity of the multifunctional material during the SE-SRE period in this test was 3.19 $mol \cdot kg^{-1} \cdot h^{-1}$. The thermal efficiency during the prebreakthrough period was found as 0.74, which is higher than the result (0.71) obtained from SE-SRE with a Ni-HTlc material in one of our previous study.[14]

However, regeneration is required after SE-SRE reaction, and the thermal efficiency of the whole process will decrease due to the use of steam (the latent energy of water). The carbon dioxide desorption method of the sorbent can be found from section 3.3 and Table 5. The regeneration took around 1200 s until $\dot{n}_{CO_2,out} \leq 0.1$ $mmol \cdot min^{-1}$, and the thermal efficiency decreased from 0.74 to 0.52 after 0.088 mol (~1.6 mL) of water was fed into the reactor to regenerate the sorbent.

Due to the steam required for sorbent regeneration, thermal efficiency (0.52) of the overall SE-SRE is only slightly higher than thermal efficiency of a conventional SRE process[14] (0.51). However, numerous separation steps are required to produce pure H_2 from product gas mixture produced in a conventional reforming process, which can greatly increase the cost and reduce the efficiency. Besides, recycling of excess energy from the outlet stream during regeneration has not been considered. Therefore, in comparison with a conventional reforming process, better energy efficiency can be achieved with SE-SRE.

Comparing Figure 8b with Figure 9a, we find that, at a temperature of 773 K, the higher the reactant mixture feeding rates, the shorter the breakthrough times during SE-SRE. These breakthrough times were very important for design of a SE-SRE process to employ this hybrid material for hydrogen production. In the design of a cyclic SE-SRE process, the longer the prebreakthrough period, the less parallel columns would be required for a continuous operation, which can be an advantage in the fixed construction cost.[14] Therefore, a detailed investigation will be carried out in the near future to design a cyclic SE-SRE operation process with the material synthesized in this work.

4. CONCLUSION

A novel multifunctional hybrid material was synthesized with multivalent properties, catalytic activity, and selectivity, as well as selective sorption toward carbon dioxide for SE-SRE. The catalytic behavior obtained for SRE was investigated and found to be more promising than the previously used HTlc materials incorporated with Ni or Cu alone. The multifunctional hybrid material used in this work kept a similar carbon dioxide adsorption capacity as the K-promoted hydrotalcite studied in former studies. It is found that the K−HTlc structure was kept in the multiphase material, similarly to previously used individual materials. In this work, the formation of a nickel−copper alloy phase has been observed, which can be very helpful for catalytic properties due to the formation of small ensembles of nickel and copper that reduce in considerable amount the interactions of adsorbed species on the specific metallic surfaces. The metallic crystallite size of the $Ni_{0.5}Cu_{0.5}$ alloy was found to be very small, which has the benefit of high catalytic activity. The hybrid material consisting of multiple phase composition used for SRE was found to have promising activity and selectivity, together with excellent selective carbon dioxide sorption capacity. This multifunctional material is one of the most promising SERP materials, which is ripe for a scale-up SE-SRE process design to produce high-purity hydrogen in a single reaction unit.

AUTHOR INFORMATION

Corresponding Author

*E-mail: afcunha@fe.up.pt. Telephone: +351-22-5081671. Fax: +351-22-5081674.

Notes

The authors declare no competing financial interest.

ACKNOWLEDGMENTS

A.F.C. is grateful to Fundação para a Ciência e Tecnologia (FCT), Portugal, for providing financial support for this research program and for postdoctoral grant SFRH/BPD/62968/2009. Y.-J.W. gratefully acknowledges a doctoral grant from China Scholarship Council (2010674011). This work was cofinanced by QREN, ON2, and FEDER (Project NORTE-07-0124-FEDER-0000007).

ABBREVIATIONS

ACD = acetaldehyde decomposition
ETD = ethanol decomposition
HTlc = hydrotalcite-like compound
LDH = layered double hydroxide
SERP = sorption-enhanced reaction process
SE-SRE = sorption-enhanced steam reforming of ethanol
SMR = steam methane reforming
SRE = steam reforming of ethanol
WGS = water−gas shift

REFERENCES

(1) Doman, L. E. *International Energy Outlook 2013*; U.S. Energy Information Administration, Washington, DC, 2013.
(2) Barreto, L.; Makihira, A.; Riahi, K. The hydrogen economy in the 21st century: a sustainable development scenario. *Int. J. Hydrogen Energy* **2003**, *28* (3), 267−284.
(3) Liu, K.; Song, C.; Subramani, V. *Hydrogen and syngas production and purification technologies*; Wiley: Hoboken, NJ, 2010.

(4) Wang, Z.; Wang, H.; Liu, Y. $La_{1-x}Ca_xFe_{1-x}Co_xO_3$: A stable catalyst for oxidative steam reforming of ethanol to produce hydrogen. *RSC Adv.* **2013**, *3* (25), 10027−10036.
(5) Chakrabarti, R.; Kruger, J. S.; Hermann, R. J.; Schmidt, L. D. Autothermal reforming of isobutanol. *RSC Adv.* **2012**, *2* (6), 2527−2533.
(6) Ferreira-Aparicio, P.; Benito, M. J.; Sanz, J. L. New trends in reforming technologies: from hydrogen industrial plants to multifuel microreformers. *Catal. Rev.: Sci. Eng.* **2005**, *47* (4), 491−588.
(7) Espinal, R.; Taboada, E.; Molins, E.; Chimentao, R. J.; Medina, F.; Llorca, J. Cobalt hydrotalcite for the steam reforming of ethanol with scarce carbon production. *RSC Adv.* **2012**, *2* (7), 2946−2956.
(8) Wu, Y. J.; Santos, J.; Li, P.; Yu, J. G.; Cunha, A.; Rodrigues, A. Simplified kinetic model for steam reforming of ethanol on a Ni/Al_2O_3 catalyst. *Can. J. Chem. Eng.* **2014**, *92* (1), 116−130.
(9) Divisek, J.; Oetjen, H. F.; Peinecke, V.; Schmidt, V. M.; Stimming, U. Components for PEM fuel cell systems using hydrogen and CO containing fuels. *Electrochim. Acta* **1998**, *43* (24), 3811−3815.
(10) Hufton, J.; Mayorga, S.; Sircar, S. Sorption-enhanced reaction process for hydrogen production. *AIChE J.* **1999**, *45* (2), 248−256.
(11) Xiu, G.-h.; Li, P.; E Rodrigues, A. Sorption-enhanced reaction process with reactive regeneration. *Chem. Eng. Sci.* **2002**, *57* (18), 3893−3908.
(12) Harrison, D. P. Sorption-enhanced hydrogen production: a review. *Ind. Eng. Chem. Res.* **2008**, *47* (17), 6486−6501.
(13) Cunha, A. F.; Wu, Y. J.; Díaz Alvarado, F. A.; Santos, J. C.; Vaidya, P. D.; Rodrigues, A. E. Steam reforming of ethanol on a Ni/Al_2O_3 catalyst coupled with a hydrotalcite-like sorbent in a multilayer pattern for CO_2 uptake. *Can. J. Chem. Eng.* **2012**, *90* (6), 1514−1526.
(14) Wu, Y. J.; Li, P.; Yu, J. G.; Cunha, A. F.; Rodrigues, A. E. Sorption-enhanced steam reforming of ethanol on NiMgAl multifunctional materials: experimental and numerical investigation. *Chem. Eng. J.* **2013**, *231*, 36−48.
(15) Halabi, M. H.; de Croon, M. H. J. M.; van der Schaaf, J.; Cobden, P. D.; Schouten, J. C. Kinetic and structural requirements for a CO_2 adsorbent in sorption enhanced catalytic reforming of methane − Part I: Reaction kinetics and sorbent capacity. *Fuel* **2012**, *99* (0), 154−164.
(16) Kim, J.-N.; Ko, C. H.; Yi, K. B. Sorption enhanced hydrogen production using one-body $CaO−Ca_{12}Al_{14}O_{33}$−Ni composite as catalytic absorbent. *Int. J. Hydrogen Energy* **2013**, *38* (14), 6072−6078.
(17) Feng, H. Z.; Lan, P. Q.; Wu, S. F. A study on the stability of a $NiO−CaO/Al_2O_3$ complex catalyst by La_2O_3 modification for hydrogen production. *Int. J. Hydrogen Energy* **2012**, *37* (19), 14161−14166.
(18) Nahil, M. A.; Wang, X.; Wu, C.; Yang, H.; Chen, H.; Williams, P. T. Novel bi-functional Ni-Mg-Al-CaO catalyst for catalytic gasification of biomass for hydrogen production with in situ CO_2 adsorption. *RSC Adv.* **2013**, *3* (16), 5583−5590.
(19) Wang, Q.; Gao, Y.; Luo, J.; Zhong, Z.; Borgna, A.; Guo, Z.; O'Hare, D. Synthesis of nano-sized spherical Mg_3Al-CO_3 layered double hydroxide as a high-temperature CO_2 adsorbent. *RSC Adv.* **2013**, *3* (10), 3414−3420.
(20) Andersson, M. P.; Abild-Pedersen, F.; Remediakis, I. N.; Bligaard, T.; Jones, G.; Engbæk, J.; Lytken, O.; Horch, S.; Nielsen, J. H.; Sehested, J.; Rostrup-Nielsen, J. R.; Nørskov, J. K.; Chorkendorff, I. Structure sensitivity of the methanation reaction: H_2-induced CO dissociation on nickel surfaces. *J. Catal.* **2008**, *255* (1), 6−19.
(21) Zhang, C.; Zhang, P.; Li, S.; Wu, G.; Ma, X.; Gong, J. Superior reactivity of skeletal Ni-based catalysts for low-temperature steam reforming to produce CO-free hydrogen. *Phys. Chem. Chem. Phys.* **2012**, *14* (10), 3295−3298.
(22) Poggio-Fraccari, E.; Mariño, F.; Laborde, M.; Baronetti, G. Copper and nickel catalysts supported on praseodymium-doped ceria (PDC) for the water-gas shift reaction. *Appl. Catal., A* **2013**, *460−461*, 15−20.
(23) Cunha, A. F.; Wu, Y. J.; Santos, J. C.; Rodrigues, A. E. Sorption enhanced steam reforming of ethanol on hydrotalcite-like compounds impregnated with active copper. *Chem. Eng. Res. Des.* **2013**, *91* (3), 581−592.
(24) Cunha, A. F.; Wu, Y.-J.; Santos, J. C.; Rodrigues, A. E. Steam reforming of ethanol on copper catalysts derived from hydrotalcite-like materials. *Ind. Eng. Chem. Res.* **2012**, *51* (40), 13132−13143.
(25) Wu, Y. J.; Li, P.; Yu, J. G.; Cunha, A. F.; Rodrigues, A. E. K-promoted hydrotalcites for CO_2 capture in sorption enhanced reactions. *Chem. Eng. Technol.* **2013**, *36* (4), 567−574.
(26) Sasol product information, www.sasoltechdata.com/tds/Pural-MG.pdf.
(27) Rostrup-Nielsen, J. R.; Hojlund, N. *Deactivation and Poisoning of Catalysts*; Taylor & Francis: New York, 1985.
(28) Nakano, H.; Ogawa, J.; Nakamura, J. Growth mode of carbide from C_2H_4 or CO on Ni(111). *Surf. Sci.* **2002**, *514* (1−3), 256−260.
(29) Mariño, F.; Boveri, M.; Baronetti, G.; Laborde, M. Hydrogen production from steam reforming of bioethanol using $Cu/Ni/K/\gamma-Al_2O_3$ catalysts. Effect of Ni. *Int. J. Hydrogen Energy* **2001**, *26* (7), 665−668.
(30) Da Costa-Serra, J. F.; Navarro, M. T.; Rey, F.; Chica, A. Bioethanol steam reforming on Ni-based modified mordenite. Effect of mesoporosity, acid sites and alkaline metals. *Int. J. Hydrogen Energy* **2012**, *37* (8), 7101−7108.
(31) Mariño, F.; Baronetti, G.; Jobbagy, M. A.; Laborde, M. Cu-Ni-$K/\gamma-Al_2O_3$ supported catalysts for ethanol steam reforming: Formation of hydrotalcite-type compounds as a result of metal−support interaction. *Appl. Catal., A* **2003**, *238* (1), 41−54.
(32) Chen, L.-C.; Lin, S. D. The ethanol steam reforming over $Cu-Ni/SiO_2$ catalysts: Effect of Cu/Ni ratio. *Appl. Catal., B* **2011**, *106* (3−4), 639−649.
(33) Oliveira, E. L. G.; Grande, C. A.; Rodrigues, A. E. CO_2 sorption on hydrotalcite and alkali-modified (K and Cs) hydrotalcites at high temperatures. *Sep. Purif. Technol.* **2008**, *62* (1), 137−147.
(34) Carrado, K. A.; Csencsits, R.; Thiyagarajan, P.; Seifert, S.; Macha, S. M.; Harwood, J. S. Crystallization and textural porosity of synthetic clay minerals. *J. Mater. Chem.* **2002**, *12* (11), 3228−3237.
(35) Ban, I.; Stergar, J.; Drofenik, M.; Ferk, G.; Makovec, D. Synthesis of copper−nickel nanoparticles prepared by mechanical milling for use in magnetic hyperthermia. *J. Magn. Magn. Mater.* **2011**, *323* (17), 2254−2258.
(36) Bonet, F.; Grugeon, S.; Dupont, L.; Herrera Urbina, R.; Guéry, C.; Tarascon, J. M. Synthesis and characterization of bimetallic Ni−Cu particles. *J. Solid State Chem.* **2003**, *172* (1), 111−115.
(37) Cunha, A. F.; Órfão, J. J. M.; Figueiredo, J. L. Methane decomposition on Ni−Cu alloyed Raney-type catalysts. *Int. J. Hydrogen Energy* **2009**, *34* (11), 4763−4772.
(38) Wu, Y.-J.; Díaz Alvarado, F.; Santos, J. C.; Gracia, F.; Cunha, A. F.; Rodrigues, A. E. Sorption-enhanced steam reforming of ethanol: Thermodynamic comparison of CO_2 sorbents. *Chem. Eng. Technol.* **2012**, *35* (5), 847−858.
(39) Díaz Alvarado, F.; Gracia, F. Steam reforming of ethanol for hydrogen production: Thermodynamic analysis including different carbon deposits representation. *Chem. Eng. J.* **2010**, *165* (2), 649−657.
(40) Natter, H.; Schmelzer, M.; Hempelmann, R. Nanocrystalline nickel and nickel-copper alloys: Synthesis, characterization, and thermal stability. *J. Mater. Res.* **1998**, *13* (5), 1186−1197.
(41) Moulijn, J. A.; van Diepen, A. E.; Kapteijn, F. Catalyst deactivation: Is it predictable? What to do? *Appl. Catal., A* **2001**, *212* (1−2), 3−16.
(42) Erickson, K. L.; Bostrom, T. E.; Frost, R. L. A study of structural memory effects in synthetic hydrotalcites using environmental SEM. *Mater. Lett.* **2005**, *59* (2−3), 226−229.
(43) Mas, V.; Kipreos, R.; Amadeo, N.; Laborde, M. Thermodynamic analysis of ethanol/water system with the stoichiometric method. *Int. J. Hydrogen Energy* **2006**, *31* (1), 21−28.
(44) Mariño, F.; Boveri, M.; Baronetti, G.; Laborde, M. Hydrogen production via catalytic gasification of ethanol. A mechanism proposal over copper−nickel catalysts. *Int. J. Hydrogen Energy* **2004**, *29* (1), 67−71.

(45) Ampelli, C.; Passalacqua, R.; Genovese, C.; Perathoner, S.; Centi, G.; Montini, T.; Gombac, V.; Delgado, J. J.; Fornasiero, P. H_2 production by selective photo-dehydrogenation of ethanol in gas and liquid phase on CuO_x/TiO_2 nanocomposites. *RSC Adv.* **2013**, *3*, 21776−21788.
(46) Li, Y.; Fu, Q.; Flytzani-Stephanopoulos, M. Low-temperature water-gas shift reaction over Cu- and Ni-loaded cerium oxide catalysts. *Appl. Catal., B* **2000**, *27* (3), 179−191.
(47) Ebiad, M. A.; Abd El-Hafiz, D. R.; Elsalamony, R. A.; Mohamed, L. S. Ni supported high surface area CeO_2-ZrO_2 catalysts for hydrogen production from ethanol steam reforming. *RSC Adv.* **2012**, *2* (21), 8145−8156.
(48) Ponec, V. Catalysis by alloys in hydrocarbon reactions. *Adv. Catal.* **1983**, *32* (1), 149−214.
(49) Wijngaarden, R. I.; Westerterp, K. R.; Kronberg, A.; Bos, A. *Industrial catalysis: optimizing catalysts and processes*; Wiley−VCH: Weinheim, Germany, 1998.
(50) Xu, J.; Zhang, X.; Zenobi, R.; Yoshinobu, J.; Xu, Z.; Yates, J. T., Jr. Ethanol decomposition on Ni(111): Observation of ethoxy formation by IRAS and other methods. *Surf. Sci.* **1991**, *256* (3), 288−300.
(51) Hagen, J. *Industrial Catalysis: A Practical Approach*; Wiley−VCH: Weinheim, Germany, 2006.
(52) Bartholomew, C. H. Mechanisms of catalyst deactivation. *Appl. Catal., A* **2001**, *212* (1−2), 17−60.
(53) Ding, Y.; Alpay, E. Equilibria and kinetics of CO_2 adsorption on hydrotalcite adsorbent. *Chem. Eng. Sci.* **2000**, *55* (17), 3461−3474.
(54) Cavani, F.; Trifirò, F.; Vaccari, A. Hydrotalcite-type anionic clays: Preparation, properties and applications. *Catal. Today* **1991**, *11* (2), 173−301.
(55) Rawadieh, S.; Gomes, V. G., Catalyst-adsorbent configurations in enhancing adsorptive reactor performance. *Int. J. Chem. React. Eng.* **2007**, *5* (1).
(56) Rawadieh, S.; Gomes, V. G. Steam reforming for hydrogen generation with in situ adsorptive separation. *Int. J. Hydrogen Energy* **2009**, *34* (1), 343−355.
(57) Lu, Z. P.; Rodrigues, A. E. Pressure swing adsorption reactors: Simulation of three-step one-bed process. *AIChE J.* **1994**, *40* (7), 1118−1137.
(58) Chanburanasiri, N.; Ribeiro, A. M.; Rodrigues, A. E.; Arpornwichanop, A.; Laosiripojana, N.; Praserthdam, P.; Assabumrungrat, S. Hydrogen production via sorption enhanced steam methane reforming process using Ni/CaO multifunctional catalyst. *Ind. Eng. Chem. Res.* **2011**, *50* (24), 13662−13671.
(59) He, L.; Berntsen, H.; Chen, D. Approaching sustainable H_2 production: Sorption enhanced steam reforming of ethanol. *J. Phys. Chem. A* **2009**, *114* (11), 3834−3844.
(60) Essaki, K.; Muramatsu, T.; Kato, M. Effect of equilibrium-shift in the case of using lithium silicate pellets in ethanol steam reforming. *Int. J. Hydrogen Energy* **2008**, *33* (22), 6612−6618.